Am J Physiol Cell Physiol 318: C1005–C1017, 2020.
First published April 1, 2020; doi:10.1152/ajpcell.00520.2019.

RESEARCH ARTICLE

Irradiation-induced senescence of bone marrow mesenchymal stem cells aggravates osteogenic differentiation dysfunction via paracrine signaling

Jiangtao Bai, Yuyang Wang, Jianping Wang, Jianglong Zhai, Feilong He, and Guoying Zhu

Department of Radiation Health, Institute of Radiation Medicine, Fudan University, Shanghai, China

Submitted 15 November 2019; accepted in final form 24 March 2020

Bai J, Wang Y, Wang J, Zhai J, He F, Zhu G. Irradiation-induced senescence of bone marrow mesenchymal stem cells aggravates osteogenic differentiation dysfunction via paracrine signaling. *Am J Physiol Cell Physiol* 318: C1005–C1017, 2020. First published April 1, 2020; doi:10.1152/ajpcell.00520.2019.—The role of cellular senescence induced by radiation in bone loss has attracted much attention. As one of the common complications of anticancer radiotherapy, irradiation-induced bone deterioration is common and clinically significant, but the pathological mechanism has not been elucidated. This study was performed to explore the cellular senescence and senescence-associated secretory phenotype (SASP) induction of bone marrow-derived mesenchymal stem cells (BMSCs) by irradiation and its role in osteogenic differentiation dysfunction. It was observed that irradiated BMSCs lost typical fibroblast-like morphology, exhibited suppressed viability and differentiation potential accompanied with senescence phenotypes, including an increase in senescence-associated β-galactosidase (SA-β-gal) staining-positive cells, and upregulated senescence-related genes *p53/p21*, whereas no changes happened to *p16*. Additionally, DNA damage γ-H2AX foci, G0/G1 phase of cell cycle arrest, and cellular and mitochondrial reactive oxygen species (ROS) increased in an irradiation dose-dependent manner. Meanwhile, the JAK1/STAT3 pathway was activated and accompanied by an increase in SASP secretion, such as IL-6, IL-8, and matrix metalloproteinase-9 (MMP9), whereas 0.8 μM JAK1 inhibitor (JAKi) treatment effectively inhibited the JAK pathway and SASP production. Furthermore, conditioned medium (CM) from irradiation-induced senescent (IRIS) BMSCs exhibited a markedly reduced ability in osteogenic differentiation and marker gene expression of osteoblasts, whereas CM with JAKi intervention may effectively improve these deterioration effects. In conclusion, irradiation could provoke BMSC senescence and SASP secretion and further aggravate osteogenic differentiation dysfunction via paracrine signaling, whereas SASP targeting may be a possible intervention strategy for alleviating irradiation-induced bone loss.

bone marrow mesenchymal stem cells; cellular senescence; irradiation; osteogenic differentiation; SASP

INTRODUCTION

With cancer incidence rising, radiotherapy has become widely used in anticancer treatment. Although radiotherapy technology has been developing continuously, patients still inevitably suffer from a certain degree of damage to surrounding normal tissue. Irradiation-induced bone loss has been a challenge for many years, especially among patients with cancer undergoing radiotherapy, who suffer from a high risk of fracture (9, 36, 37, 39). Specific evidence for the adverse side effects of irradiation on the bone system was observed in patients who received radiotherapy for urinary and gynecologic tumors, and the incidence of postradiation pelvic insufficiency fractures (PIFs) was up to 10–29%, predominantly in the hips, which may cause refractory pain and impair the life quality of the patients (38). Similarly, astronauts who participate in long-duration flight are unavoidably exposed to space radiation and have a considerable bone loss of 1–2% of bone mass per month in flight, occurring mainly in the load-bearing parts of the lumbar spine and legs. Even 6 mo after landing, damage to the trabecular region has not been recovered (22). Thus it can be seen that irradiation-induced bone loss has long been an urgent challenge. However, the underlying pathological mechanisms have not yet been elucidated because of its multicellular regulation in bone tissue.

Historical studies have demonstrated that ionizing radiation, a significant factor that could directly cause a high level of DNA damage and oxidative stress, can lead to cellular apoptosis and senescence in vivo and in vitro. In the radiotherapy for the keloid, previous studies have suggested that X-ray radiation can prevent the recurrence of keloid by cell cycle arrest and premature cell senescence (6, 19, 24). On the other hand, irradiation-induced cell and tissue senescence is more likely to play a crucial role in the pathogenesis of many diseases. For example, animal studies have shown that acute postnatal exposure to ≥0.1 Gy may significantly induce cognitive impairment and aging (31). Therefore, we speculate that the cellular senescence in bone tissue induced by irradiation may be one of the important mechanisms of irradiation-induced bone loss. Although extensive studies have been conducted on the oxidative stress and DNA damage in irradiation-induced bone loss, the role of cellular senescence, one of the worst endings, is still unclear. It has been clearly understood that oxidative stress and DNA damage are key factors in triggering cellular senescence (6) and that the pathophysiology of irradiation-induced bone loss is very similar to age-related osteoporosis: both have similar pathological changes such as osteogenic dysfunction of bone marrow-derived mesenchymal stem cells (BMSCs), increase of bone marrow fat, dysfunction and reduction of osteoblasts on the bone surface, and osteocyte apoptosis (2, 3, 16). In this study, we aimed to investigate the irradiation-induced cellular senescence phenotype and senescence-associated secretory phenotype (SASP) induction, to explore its role in osteogenic dysfunction as a pathological mechanism of irradiation-induced bone loss.

Correspondence: G. Zhu (e-mail: zhugy@shmu.edu.cn).

MATERIALS AND METHODS

BMSC isolation and culture. Primary BMSCs were isolated from 4-wk-old male Sprague–Dawley rats (weight ~100 g) purchased from the Department of Experimental Animals at Fudan University (Shanghai, China). All experimental procedures were approved by the Committee for Ethical Use of Experimental Animals at Fudan University. Cervical dislocation was used by the professional experimenter for rat euthanasia, and then the femurs and tibiae were dislocated immediately after euthanasia. The animal remains were frozen and sent to the relevant department for disposal. Muscles and connective tissue were stripped subsequently, whereafter total bone marrow cells were flushed by phosphate-buffered saline (PBS) and dissociated into single-cell suspension with complete medium. After the suspension was centrifuged at 1,000 rpm for 10 min at 20°C, cells were resuspended with α-minimum essential medium (α-MEM; GIBCO) containing 10% fetal bovine serum (FBS; GIBCO) and 1% penicillin-streptomycin (GIBCO) and seeded for incubation in a humidified incubator containing 5% CO_2 at 37°C. Tightly adhered cells were collected as BMSCs after 48-h culture.

Antibodies. CD29 (bs-0486R-FITC), CD44 (bs-0521R-FITC), CD34 (bs-0646R), osteocalcin (OC; bs-0470R), and alkaline phosphatase (ALP; bs-6292R) were purchased from Bioss Technology (Beijing, China). CD45 (11-0461-80) was purchased from Thermo Fisher Scientific (Waltham, MA). γ-H2AX (phospho-S139) primary antibody (ab81299) and rabbit monoclonal antibodies against p53 (ab131442), p21 (ab109199), and p16 (ab51243) were purchased from Abcam (Cambridge, MA). Mouse monoclonal antibody against β-actin (AF7018), peroxisome proliferator-activated receptor-γ (PPAR-γ; AF6284), Runx2 (AF5186), phospho-JAK1 (Tyr1022/Tyr1023) (AF2012), STAT3 (AF6294), and phospho-STAT3 (Tyr705) (AF3293) were purchased from Affinity Biosciences (Cincinnati, OH). FITC-labeled goat-rabbit IgG (A0562) and anti-rabbit and anti-mouse antibodies (A0208 and A0216) were purchased from Beyotime Biotechnology (Shanghai, China).

Surface marker detection. BMSCs at *passage 3* were harvested to detect surface antigens by flow cytometry, including CD29, CD44, CD34, and CD45. Briefly, after digestion and centrifugation, BMSCs were incubated with anti-CD44-FITC (1:200), anti-CD29-FITC (1:200), anti-CD34-FITC (1:200), and anti-CD45-FITC (1:200) conjugated antibodies separately at 4°C in the dark for 30 min. After incubation, the cells were washed with PBS and tested by a flow cytometer (Beckman Coulter, Miami, FL).

BMSC irradiation exposure. Sixty to seventy percent confluence BMSCs were irradiated with increasing doses (0 Gy, 2 Gy, 5 Gy, and 10 Gy) of ^{137}Cs gamma rays (Nordion, Ottawa, ON, Canada). Nonirradiated (0-Gy) cells were placed in the irradiator for the same period without radiation. After irradiation, all cells were replaced with fresh medium, cultured for another 2 days, and then seeded for the subsequent experiments.

BMSC differentiation assay. The *passage 3* BMSCs were seeded and cultured with osteogenic induction medium [α-MEM supplemented with 15% FBS, 1% penicillin-streptomycin, 50 mg/L ascorbic acid, 10^{-8} M dexamethasone (Sigma-Aldrich), and 10 mmol/L β-glycerol phosphate (China Pharmaceutical Shanghai Chemical Reagent Co., Ltd.)] for 7 days, and then alkaline phosphatase (ALP) was detected. Additionally, the induction process continued for another 2 wk to evaluate the mineralization potential. For adipogenic differentiation, BMSCs were cultured with adipogenic induction medium [α-MEM supplemented with 15% FBS, 1% penicillin-streptomycin, 0.5 mM 3-isobutyl-1-methylxanthine (I8450; Solarbio), 0.1 mM indomethacin (YZ-100258; Solarbio), 10^{-6} M dexamethasone, and 10 μg/mL insulin (I8830; Solarbio)] for 16 days. The medium was changed every 2 days.

Alkaline phosphatase activity assay. BMSCs were seeded in 48-well plates at a density of 5×10^4 cells per well or in 96-well plates at a density of 3×10^3 cells per well. On the seventh day of osteogenic induction, cells in 48-well plates were fixed with 2.5% glutaraldehyde (Sigma-Aldrich) for 5 min and stained with BCIP/NBT Alkaline Phosphatase Color Development Kit (C3206; Beyotime Biotechnology) for 30 min at 37°C. ALP-positive cells were stained purple or blue, and images were captured to observe ALP staining. Meanwhile, cells in 96-well plates were lysed by 100 μL 0.05% Triton X-100 (T8200; Solarbio) for 2 h at 4°C, followed by ultrasonic oscillation for 3×10 s on ice. Fifty microliters of lysate were mixed with 150 μL detection buffer [diethanolamine and *p*-nitrophenyl phosphate (PNPP) at a ratio of 2:1] for 30 min at 37°C. At the end point, 50 μL NaOH (0.2 mol/L) were added to stop the reaction, and the absorbance at 405 nm was measured to calculate the ALP activity from the *p*–nitrophenol standard curve. ALP activity was calibrated by total cellular protein and expressed as units per milligram protein.

Alizarin red staining and Oil Red O staining. The *passage 3* BMSCs were seeded in 48-well plates at a density of 5×10^4 cells per well. After 21-day osteogenic induction, alizarin red staining was performed to count the mineralization nodules. Shortly, cells were fixed in 95% ethanol for 30 min and incubated in 0.1% Alizarin Red S (Sigma-Aldrich) solution (pH = 7.2) for 1 h at room temperature. In addition, Oil Red O (Sigma-Aldrich) staining was used to observe the positive cells through 16-day adipogenic induction. After fixation with 4% paraformaldehyde (P1110; Solarbio), cells were gently rinsed with 60% isopropanol and then stained with Oil Red O dye solution for 30 min at room temperature.

BMSC morphology and viability assay. Cells were stained with tetramethylrhodamine (TRITC)-phalloidin (CA1610; Solarbio) according to the manufacturer's instructions. Nuclei were counterstained with 4′,6-diamidino-2-phenylindole (DAPI, D212; Dojindo). The fluorescence images were captured by a Leica fluorescence microscope (Leica Microsystems, Wetzlar, Germany).

Cell Counting Kit-8 (CCK-8, CK04; Dojindo) and colony-forming unit (CFU) assay was used to evaluate cell viability. Briefly, cells (3,000 per well) were seeded into 96-well plates and then incubated with 10 μL CCK-8 for 2 h at 37°C. The absorbance at 450 nm was measured by a microplate reader (Bioteck, Italy). Meanwhile, the BMSCs were trypsinized into a 200 cells/mL single-cell suspension and evenly seeded at 5 mL into a petri dish. After 2-wk static culture, visible cell colonies were observed, fixed with methanol for 15 min, and incubated with Crystal Purple (C8470; Solarbio) for 10 min, and CFU was assayed.

Senescence-associated β-galactosidase staining. Senescent BMSCs were verified by senescence-associated β-galactosidase (SA-β-gal) staining according to the instructions of the SA-β-gal staining kit (C0602; Beyotime Biotechnology). Cells were fixed for 15 min at room temperature, rinsed with PBS, and stained (pH = 6.0) overnight at 37°C without CO_2. Six randomly chosen fields were photographed with a light microscope, and the percentage of senescent cells was calculated in a total of ~200 cells from each image.

Reactive oxygen species measurement. About 2×10^5 cells per well in 6-well plates were incubated in 10 μM 2′,7′-dichlorodihydrofluorescein diacetate (DCFH-DA, S0033; Beyotime Biotechnology) for 10 min at 37°C. Green fluorescence intensity under a fluorescence microscope represents intracellular reactive oxygen species (ROS) level. In addition, ~5×10^3 cells per well in 48-well plates were incubated in 0.5 μM MitoSOX (40741ES50; Yeasen Biotechnology) for 15 min at 37°C. Red fluorescence intensity under a fluorescence microscope labeled mitochondrial ROS.

Cell cycle analysis. Cell cycle phase was detected by a cell cycle staining kit (70-CCS01; Multi Sciences). BMSCs were harvested and fixed in 75% ethanol at −20°C for 24 h. Cells were centrifuged to remove alcohol and incubated in 1 mL DNA staining solution for 30 min at room temperature in the dark, and then the cell cycle phase of BMSCs was analyzed.

Immunofluorescence analysis of γ-H2AX foci. γ-H2AX foci, a marker of DNA damage, were assayed by immunofluorescence.

Briefly, after fixation in 2.5% glutaraldehyde, cells were blocked with blocking buffer (P0260; Beyotime Biotechnology) and incubated with γ-H2AX (phospho-S139) primary antibody (1:250), with FITC-labeled goat-rabbit IgG as the secondary antibody (1:500). Nuclei were stained with DAPI. Images of ~50 cells per sample were taken, and the number of γ-H2AX foci was calculated with Image-Pro Plus software (Media Cybernetics Inc., Rockville, MD).

Enzyme-linked immunosorbent assay. The main components of SASP by irradiation-induced senescent (IRIS) BMSCs, such as IL-6, IL-8, and matrix metalloproteinase-9 (MMP9), were measured using ELISA kits (Enzyme-Linked Biotechnology). In brief, irradiated BMSCs were cultured under normal conditions for 72 h, followed by culture in serum-free medium for another 24 h, and then the supernatant was collected for the ELISA experiment.

Conditioned medium collection. BMSCs and irradiated BMSCs were cultured for 72 h, followed by culture in serum-free medium for another 24 h, and the supernatant was extracted as conditioned medium (CM) from control BMSCs (Con CM) and CM from IRIS BMSCs (IRIS CM). For JAK1 inhibitor (JAKi) treatment, irradiated BMSCs were treated with 0.8 μM JAKi for 72 h, washed three times with PBS, and cultured with serum-free medium for another 24 h, and the supernatant was extracted as CM from irradiation-induced senescent BMSCs with JAKi intervention (IRIS/JAKi CM). The level of cytokines in the supernatant was standardized by cell number.

Osteoblast differentiation modulated by irradiation-induced senescent BMSCs. Primary osteoblasts were obtained according to previous experimental protocols (23), *passage 3* osteoblasts were cultured in low-glucose Dulbecco's modified Eagle's medium (L-DMEM; GIBCO), containing 50% Con CM, IRIS CM, IRIS/JAKi CM, or Con CM plus 0.8 μM JAKi (Con/JAKi CM), and the ALP activity and mineralization nodule capacity of osteoblasts were analyzed.

Total RNA extraction and real-time quantitative PCR. BMSCs were cultured in six-well plates, and total RNA was extracted using Simply P Total RNA Extraction Kit (BSC52S1; Bioflux). One microgram of total RNA was reverse transcribed using FastKing gDNA Dispelling RT SuperMix (KR118-02; Tiangen Biotech). The cDNA and TB Green Premix Ex Taq (RR420A; Takara Biomedical Technology) were used in 20 μL PCR reactions for quantitative PCR (qPCR) on a real-time PCR system (LightCycler 2.0; Roche Diagnostics GmbH, Mannheim, Germany). The primer sequences are shown in Table 1.

Western blot analysis. Cells were lysed in ice-cold cell lysis buffer containing protease inhibitors, and total cellular protein was quantified using the BCA Protein Assay Kit. For separation of proteins with different molecular weights, as well as the marker protein, 12.5% or 10% sodium dodecyl sulfate-polyacrylamide gel electrophoresis (PG113; Epizyme Biotech) was used, following which total protein was transferred onto polyvinylidene difluoride (PVDF) membranes (Millipore, Billerica, MA). After washing with Tris-buffered saline with 0.1% Tween 20 (TBST), the whole blot was blocked by 5% nonfat milk or BSA for 30 min at room temperature, and then we cut it into several strips for target proteins according to the prestained marker position; each complete blot with molecular marker positions is shown in the Supplemental Material (available at https://doi.org/10.6084/m9.figshare.12021798.v2). Next, the strips were incubated with primary antibodies separately, including mouse monoclonal antibody against β-actin (AF7018; Affinity Biosciences) and rabbit monoclonal antibodies against p53, p21, p16, PPAR-γ, Runx2, phospho-JAK1 (Tyr1022/Tyr1023), STAT3, phospho-STAT3 (Tyr705), OC, and ALP at 4°C overnight. After washing with TBST, the membranes were incubated with horseradish peroxidase-conjugated anti-rabbit and anti-mouse antibodies at room temperature for 1 h. Finally, the chemiluminescent Biotin-Labeled Nucleic Acid Detection Kit (D3308; Beyotime Biotechnology) was used to detect Western blot bands.

Statistical analysis. Statistical analyses of data were performed using IBM SPSS Statistics 20 and GraphPad Prism 5.01 (GraphPad Software Inc., San Diego, CA). Each experiment was repeated three times. Analyses of differences between groups were performed by Student's *t* test and one-way ANOVA. Values are presented as means ± SD with $P < 0.05$ considered to be statistically significant.

RESULTS

Identification of BMSC characterization. BMSCs were successfully collected from bone marrow and purified by differential attachment and digestion. As shown in Fig. 1, cell surface antigens (Fig. 1*A*) included positive markers CD29 (93.36%) and CD44 (85.40%) and negative markers CD34 (17.70%) and CD45 (32.56%). Typical BMSCs exhibiting spindle-shaped and fibroblast-like morphology were clearly observed (Fig. 1*B*). Furthermore, signs of osteogenic differentiation including mineralized nodules stained by Alizarin Red S, strong positive expression of alkaline phosphatase, and markers of adipogenic differentiation, namely, lipid droplets

Table 1. *Primer sequences for quantitative reverse transcription-polymerase chain reaction*

Target Gene	Forward (5′–3′)	Reverse (5′–3′)
Runx2	TGCCACCTCTGACTTCTGC	GTCAAGGGTCCGTAAAGTAG
PPAR-γ	ACGGTTGATTTCTCCAGCAT	GGACGCAGGCTCTACTTTGA
p53	GCTCCCCTGAAGACTGGATAA	ATTAGGTGACCCTGTCGCTG
p21	TGGACAGTGAGCAGTTGAGC	ACACGCTCCCAGACGTAGTT
p16	CCGAGAGGAAGGCGAACTC	GCTGCCCTGGCTAGTCTATCTG
SOD1	CCACGAGAAACAAGATGACT	GACTCAGACCACATAGGGAAT
SOD2	GGCCAAGGGAGATGTTACAA	GAACCTTGGACTCCCACAGA
CAT2	AGCCAGAAGAGAAACCCACA	TGAAAGAACAAGTCGCTGGC
IL-6	CCGTTTCTACCTGGAGTTTG	GTTTGCCGAGTAGACCTCAT
IL-8	CCCCCATGGTTCAGAAGATTG	TTGTCAGAAGCCAGCGTTCAC
TNF-α	CTCCCAGAAAAGCAAGCAAC	CGAGCAGGAATGAGAAGAGG
PAI-1	TTCCTCCACAGCCATTCTAGTCT	GAAAGGATCGGTCTAAAACCATCTC
MMP9	CGGCAAACCCTGCGTATTTC	GTTGCCCCCAGTTACAGTGA
MMP12	TGCAGCTGTCTTTGATCCAC	GCATCAATTTTTGGCCTGAT
CXCL12	CGCTCTGCATCAGTGACGGTAA	GGAAAGTCCTTTGGGCTGTTGTG
ALP	CTGAGCGCACGCGAGCAAC	GGCGTGGTTCACCCGAGTGG
OC	GAACAGACAAGTCCCACAC	GAGCTCACACACCTCCCTG
GAPDH	GGCACAGTCAAGGCTGAGAATG	ATGGTGGTGAAGACGCCAGTA

ALP, alkaline phosphatase; *CAT*, catalase; *MMP*, matrix metalloproteinase; *OC*, osteocalcin; *PPAR-γ*, peroxisome proliferator-activated receptor-γ; *SOD*, superoxide dismutase.

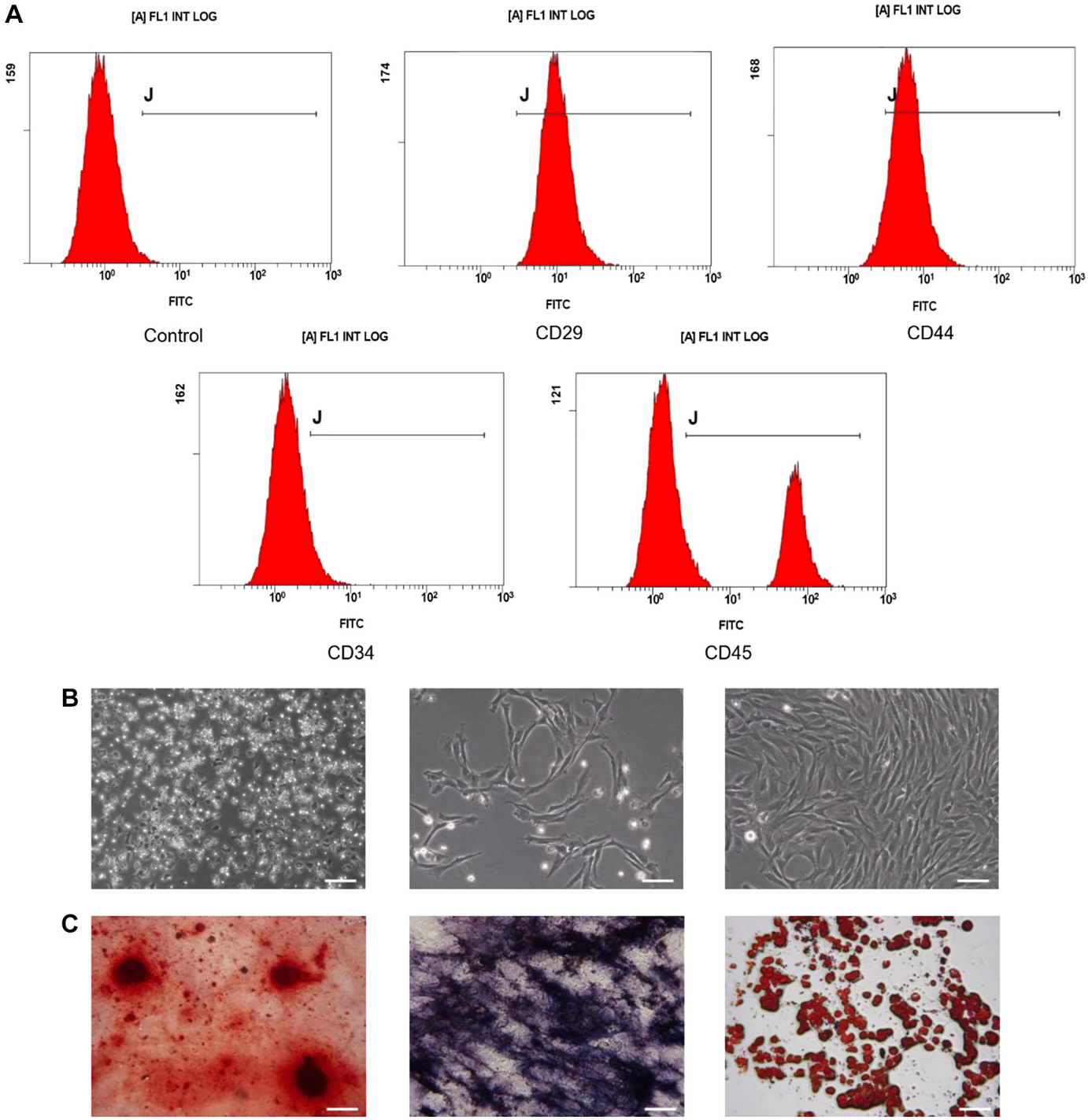

Fig. 1. Identification and multidirectional differentiation potential of primary cultured bone marrow-derived mesenchymal stem cells (BMSCs). *A*: surface markers CD29, CD44, CD34, and CD45 of primary BMSCs (1×10^6 cells per sample) extracted from bone marrow of Sprague–Dawley rats (aged 4 wk, male) were analyzed by flow cytometry. Data were analyzed from three independent experiments. J is automatically displayed in the flow cytometry system and represents the calculation area. *B*: light microscopic photographs of cells after nonadherent cells were removed and cells were cultured for 24 h and 7 days. BMSCs displayed typical fibroblast-like and whirlpool-like growth. Magnification, ×100. *C*: identification of osteogenic and adipogenic differentiation of BMSCs, including mineralized nodules stained by Alizarin Red S, positive expression of alkaline phosphatase, and lipid droplets stained by Oil Red O. Images are from three randomly obtained fields from three independent experiments. Magnification, ×100. Scale bars, 100 μm (*B* and *C*).

stained by Oil Red O (Fig. 1*C*), concurrently indicated the successful isolation and culture of BMSCs.

Damage to the biological functions of BMSCs by irradiation. Obvious morphological changes were observed in irradiated BMSCs through F-actin fluorescent staining: most BMSCs became more expanded and flatter with poor contrast under light microscopy, which closely verges on the morphology of senescent cells (Fig. 2*A*). Next, CCK-8 assay showed without a doubt that irradiation impaired cell viability, and colony formation assay also revealed the damaged self-renewal

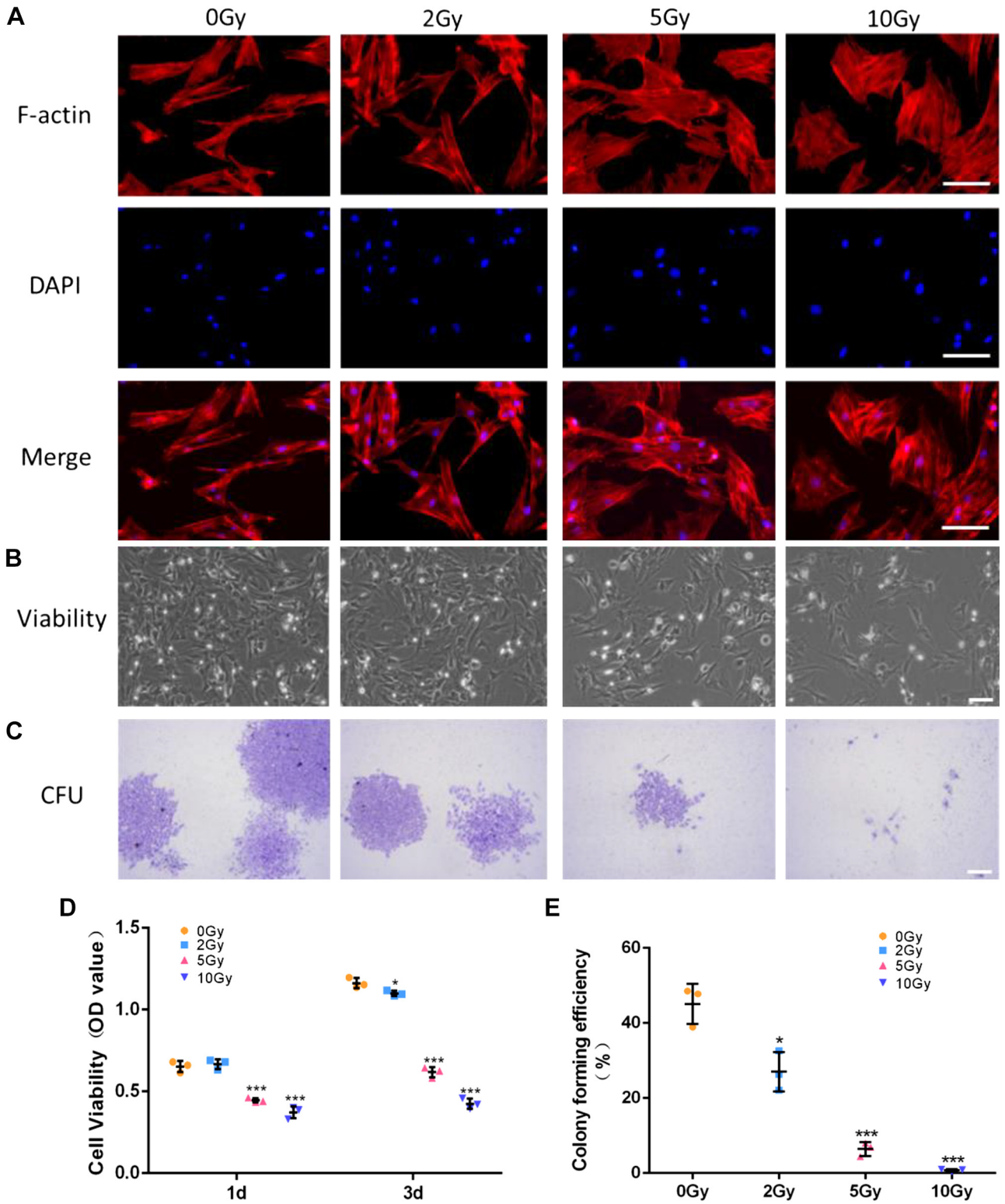

Fig. 2. Effects of gamma rays on morphology and viability of bone marrow-derived mesenchymal stem cells (BMSCs). *A*: morphological changes in BMSCs were shown after exposure to gamma rays. F-actin was stained with phalloidin, and nuclei were stained with 4′,6-diamidino-2-phenylindole (DAPI). Magnification, ×200. *B* and *D*: viability of BMSCs (3×10^3 cells per well) was suppressed immediately at 5-Gy irradiation, and on the third day the 2 Gy-irradiated BMSCs also showed a certain degree of inhibition. The cell viability was evaluated by Cell Counting Kit-8, and results are shown by optical density (OD) value. Magnification, ×100. *C* and *E*: colony-forming capacity was impaired after 2-Gy irradiation. Crystal Violet was used for staining the colonies, and the percentage of colony-forming efficiency was calculated. Images are from three randomly obtained fields from three independent experiments. Data were analyzed from three independent experiments. *P* values were calculated by Student's *t* test. Results are presented as means ± SD. Scale bars, 100 μm (*A*, *B*, and *C*). CFU, colony-forming units; d, days. Significant differences in the 2-Gy (*$P < 0.05$), 5-Gy (***$P < 0.001$), or 10-Gy (***$P < 0.001$) group compared with the 0-Gy group.

ability of BMSCs (Fig. 2, *B* and *C*). There was a mild wreck in viability and colony-forming capacity at the 2-Gy dose, whereas there was destructive reduction at 5 Gy and 10 Gy ($P < 0.05$ and $P < 0.001$, Fig. 2, *D* and *E*). Moreover, as shown in Fig. 3, *A* and *B*, an irradiation dose-dependent decrease in alkaline phosphatase activity as well as the suppression of matrix mineralization and adipogenic differentiation of BMSCs were observed. At the same time, the mRNA expression and protein level of the osteogenic differentiation-related gene *Runx2* and the adipogenic differentiation-related

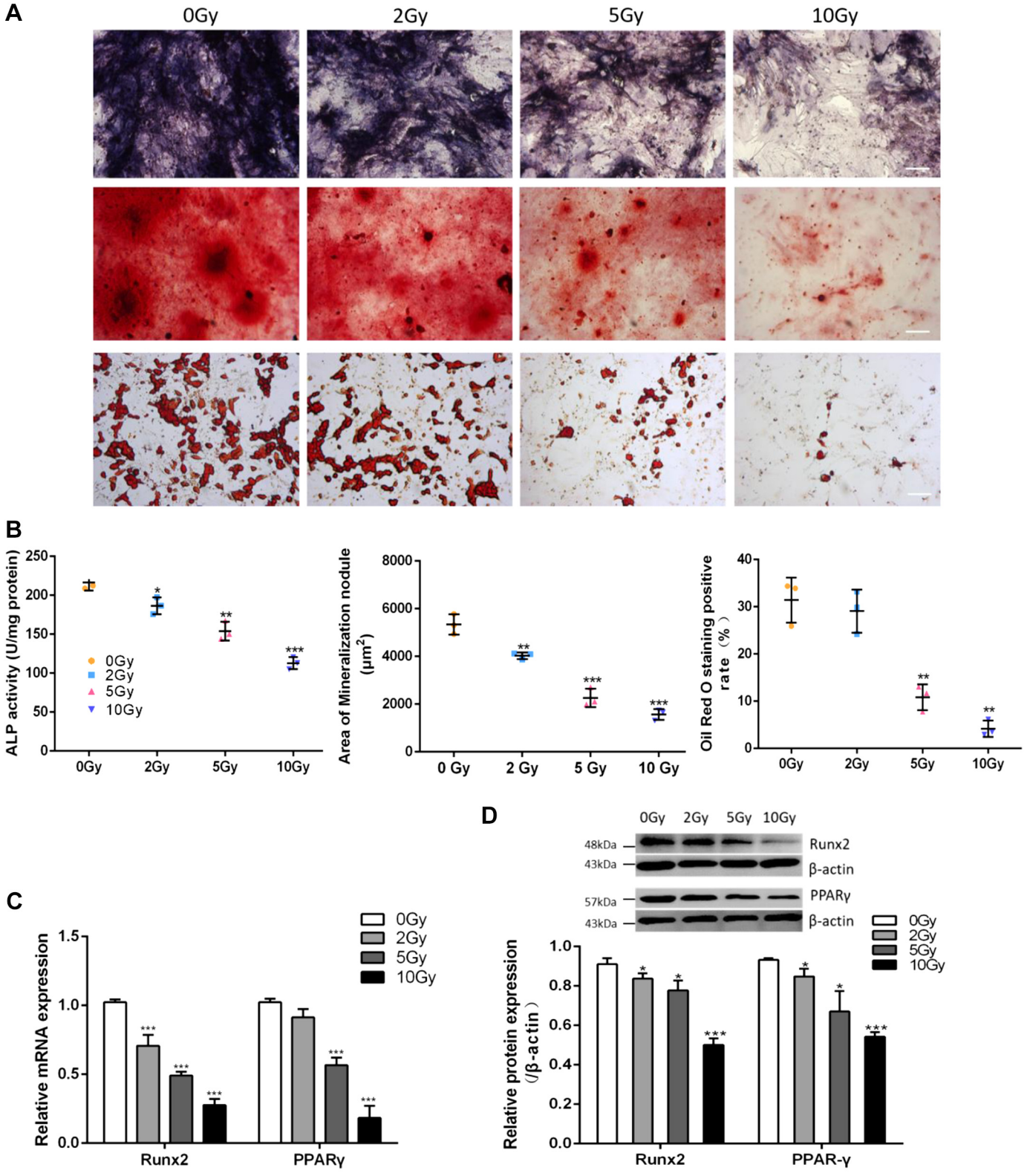

gene *PPAR*-γ both decreased in a dose-dependent manner (Fig. 3, *C* and *D*).

Senescence phenotypes and SASP secretion of BMSCs induced by irradiation. To evaluate the irradiation-induced senescence of BMSCs, SA-β-gal staining was performed first to indicate the senescent cells (Fig. 4*A*). In nonirradiated BMSCs, only 5.51 ± 2.17% cells were positive for SA-β-gal staining (blue), whereas the percentage of SA-β-gal-positive cells significantly rose to 14.44 ± 1.81% at 2 Gy, 31.94 ± 4.39% at 5 Gy, and 80.44 ± 3.25% at 10 Gy (Fig. 4*B*, $P < 0.05$, $P < 0.01$, and $P < 0.001$). Subsequently, flow cytometry showed a stable and permanent cell cycle arrest after irradiation, and the cell cycle phase distribution changed with an increased tendency in G0/G1 phase arrest, with a significant increase when the dose went up to 5 Gy and 10 Gy (Fig. 4, *C* and *D*, $P < 0.01$). Furthermore, results of the mRNA and protein levels of senescence-related genes showed that irradiation caused upregulation of *p53* and *p21* from 2 Gy to 10 Gy, whereas *p16* had no obvious change at any dose of gamma rays (Fig. 4, *E–G*, $P < 0.05$ and $P < 0.01$). What is more, the expression of multiple SASP components was gradually upregulated as the irradiation dose increased; especially, *PAI-1*, *MMP9*, and *MMP12* showed a more obvious increase at 5 Gy and 10 Gy (Fig. 4*H*). ELISA results (Fig. 4*I*, $P < 0.01$ and $P < 0.001$) also showed increased levels of several specific SASP components in the cell supernatant, such as IL-6, IL-8, and MMP9. Taken together, these results fully demonstrate that irradiation induced senescence phenotypes of BMSCs and SASP induction in a dose-dependent manner.

Induction of DNA damage and oxidative stress and activation of the JAK1/STAT3 pathway by irradiation. To investigate the underlying mechanisms by which irradiation induced cellular senescence of BMSCs, DNA damage and oxidative stress were analyzed. Since irradiation can directly cause DNA damage in cells, we first detected γ-H2AX, the marker of double-strand break (DSB), by immunofluorescence staining analyses. Results showed more γ-H2AX foci-positive BMSCs after irradiation than in the nonirradiation group. Specifically, not only the percentage of γ-H2AX foci-positive cells increased, but also the number of foci in each positive cell increased (Fig. 5, *A–C*). Meanwhile, the levels of cellular and mitochondrial ROS ascended markedly after irradiation, but the scavenging ability of ROS was weakened, as shown by the decreased expression of *SOD1*, *SOD2*, as well as catalase (*CAT2*; Fig. 5, *D–G*, $P < 0.05$, $P < 0.01$, and $P < 0.001$).

Since the JAK1/STAT pathway plays an important role in the regulation of cytokine production, the changes in JAK signaling proteins of irradiated BMSCs were explored. As shown in Fig. 6, *A* and *B*, it was demonstrated that the JAK1/STAT3 pathway was activated by irradiation, with upregulated expression of phosphorylated JAK1 (p-JAK1), total STAT3 (T-STAT3), and phosphorylated STAT3 (p-STAT3). The application of JAKi at a dose of 0.8 μM effectively inhibited the expression of p-JAK1, whereas the downstream phosphorylated STAT3 expression was more significantly blocked, accompanied by the reduced secretion of SASP components, including IL-6, IL-8, and MMP-9 (Fig. 6*C*). More interestingly, the osteogenic differentiation and mineralization ability (Fig. 6, *D–G*) of osteoblasts cocultured with IRIS/JAKi CM were also reversed compared with IRIS CM, along with the increased expression of *ALP* and *OC* (Fig. 6, *H* and *I*). In addition, it was observed that there was no effect on osteogenic differentiation of osteoblasts between those cocultured with Con CM and those cocultured with Con/JAKi CM.

DISCUSSION

Senescence is a key factor of degenerative diseases, such as cardiovascular disease, Alzheimer's disease, obesity-related insulin resistance diabetes, and osteoporosis (12, 18, 28). A decline in bone formation and relatively enhanced bone resorption are the principal pathophysiological mechanisms in charge of bone loss related to aging and other adverse stimulations, such as radiotherapy and chemotherapy. It is well known that BMSCs in bone marrow are a population of cells possessing bone formation potential; thus their functional status is important for the maintenance of bone health (1). BMSCs, together with osteocytes in bone, are the long-lived cells in the bone microenvironment. Evidence from multiple studies has shown that long-lived cells are more susceptible to various disadvantages that may affect cell life span and cause cellular senescence (7, 11), whereas short-lived bone cells, such as osteoblast progenitors, osteoblasts, and osteoclasts, can be continuously replenished by specific progenitor cells. Therefore, premature senescence of long-lived BMSCs and osteocytes caused by adverse factors seemingly has significantly worse impacts on bone remodeling (10, 13, 20). An age-related decrease in the proliferation and functional ability of BMSCs has been strongly considered to be the decisive cause of bone formation functional degradation (3, 13). In our study, we provide evidence that under exposure to gamma rays, BMSCs exhibited senescence phenotypes along with increased accumulation of DNA damage and ROS in vitro and, which is more important, the irradiation-induced senescent BMSCs could

Fig. 3. Effects of gamma rays on multidirectional differentiation potential of bone marrow-derived mesenchymal stem cells (BMSCs). *A*: weakened osteogenic and adipogenic differentiation potential compared with nonirradiated cells. Representative images of alkaline phosphatase (ALP) staining, mineralized nodules stained by Alizarin Red S, and lipid droplets stained by Oil Red O are displayed. Magnification, ×100. Images were from three randomly obtained fields from three independent experiments. *B*: quantification of ALP activity by the *p*-nitrophenyl phosphate (PNPP) method, mineralized nodule area, and lipid droplet formation. Data were analyzed from three independent experiments. *P* values were calculated by Student's *t* test. Results are presented as mean ± SD. Significant differences in the following: ALP activity of the 2-Gy ($^*P < 0.05$), 5-Gy ($^{**}P < 0.01$), or 10-Gy ($^{***}P < 0.001$) group compared with the 0-Gy group; area of mineralized nodules of the 2-Gy ($^{**}P < 0.01$), 5-Gy ($^{***}P < 0.001$), or 10-Gy ($^{***}P < 0.001$) group compared with the 0-Gy group; and positive rate of lipid droplet staining of the 5-Gy ($^{**}P < 0.01$) or 10-Gy ($^{**}P < 0.01$) group compared with the 0-Gy group. *C* and *D*: the messenger RNA (mRNA) and protein expression of *Runx2* and peroxisome proliferator-activated receptor-γ (*PPAR*-γ) of BMSCs under osteogenic and adipogenic differentiation treated with different doses of gamma rays was determined. Data were analyzed from three independent experiments. *P* values were calculated by Student's *t* test. Results are presented as means ± SD. Significant differences in the following: *Runx2* mRNA expression of the 2-Gy ($^{***}P < 0.001$), 5-Gy ($^{***}P < 0.001$), or 10-Gy ($^{***}P < 0.001$) group compared with the 0-Gy group; *PPAR*-γ mRNA expression of the 5-Gy ($^{***}P < 0.001$) or 10-Gy ($^{***}P < 0.001$) group compared with the 0-Gy group; and Runx2 and PPAR-γ protein expression of the 2-Gy ($^*P < 0.05$), 5-Gy ($^*P < 0.05$), or 10-Gy ($^{***}P < 0.001$) group compared with the 0-Gy group. Scale bars, 100 μm (*A*).

aggravate osteogenic differentiation dysfunction through paracrine signaling.

Cellular senescence was formally described by Hayflick and Moorhead (15); with more profound studies, it now refers to a process of permanent cell cycle arrest induced by various factors including telomerase deficiency, DNA damage, oxidative stress, oncogene mutation, and many other intrinsic or extrinsic initiations (8). These causes have a common cascade reaction, named the DNA damage response (DDR), which leads to cell cycle block via stabilization of p53 and transcriptional activation of p21, as well as the upregulation of expression of p16 and p19 and other signaling pathways (11, 35). In

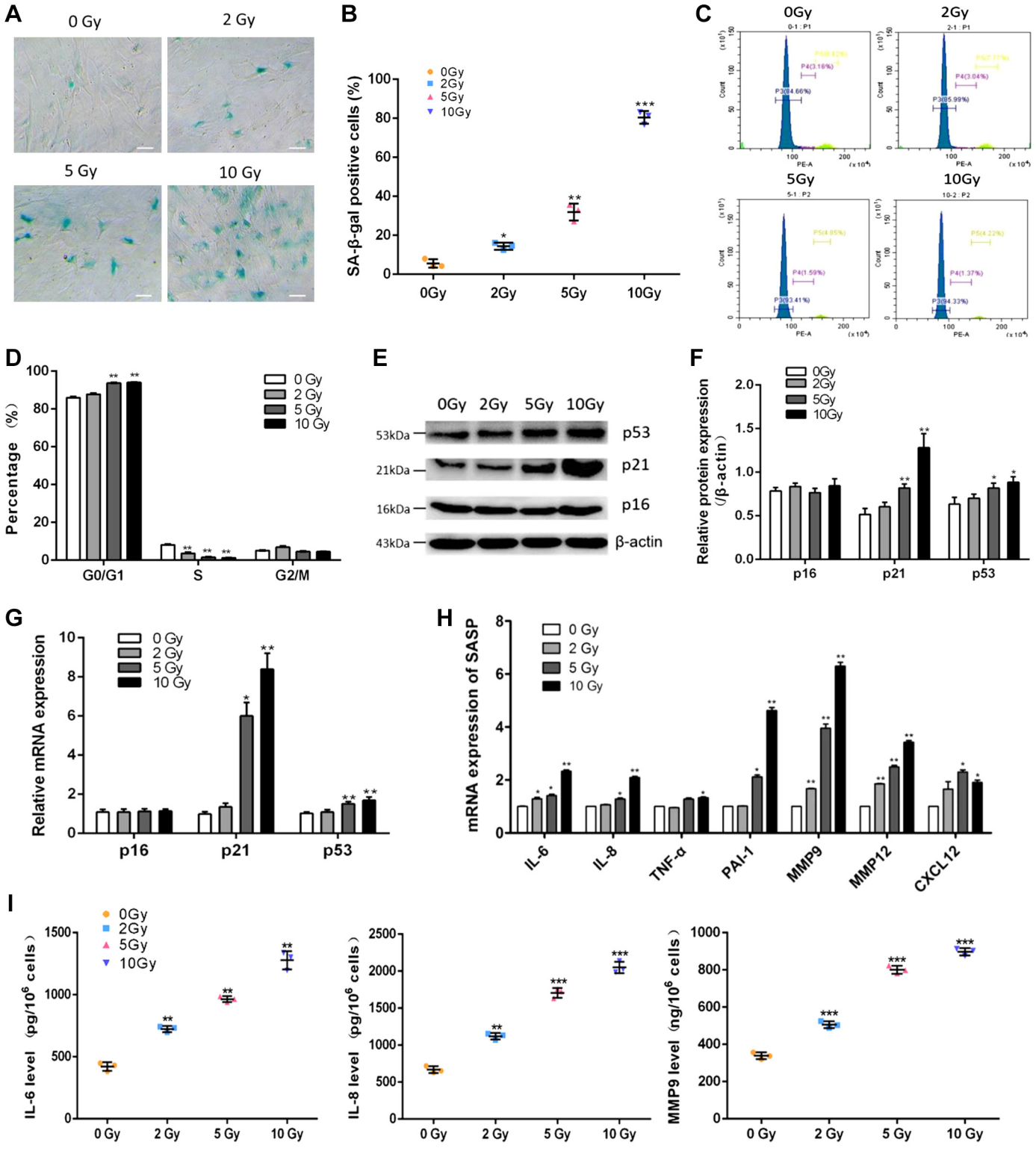

our study, the results revealed that irradiation not only impaired the biological functions of BMSCs but also induced cellular senescence and SASP induction. Specifically, irradiated BMSCs exhibited impaired viability and osteogenic differentiation. Two grays of gamma rays already had the mild ability to damage BMSCs, whereas higher doses significantly impaired the cell morphology, viability, self-renewal capacity, and differentiation potential. The results suggest that the biological functions of BMSCs can be directly damaged by irradiation in a dose-dependent manner, and the dysfunction and diminution of BMSCs postirradiation could be important causes of irradiation-induced bone deterioration, which is consistent with other studies (14, 25). Irradiation also can lead to DSB in cells, which could initiate the DDR mechanism, but if the damage fails to be repaired properly, cells may enter an irreversible damage state including mitotic catastrophe and senescence state. It is well known that γ-H2AX is an important protein marker for detecting DSB sites (29). In our study, 2 Gy of gamma rays induced detectable γ-H2AX foci, whereas higher doses of 5 Gy and 10 Gy caused more γ-H2AX foci. Similar to other studies, γ-H2AX-positive BMSCs were observed after exposure to a ^{60}Co irradiator at a dose of 6 Gy in a short period of time (33). Additionally, irradiation induced increased production of ROS, including cellular ROS and mitochondrial ROS, which suggests that oxidative stress induced by irradiation could also be a key factor inducing cellular senescence.

Senescence-related phenotypes vary according to the process of cellular senescence, including the initial, early, and late phases (17). In our study, it has been shown that senescence-related genes *p53* and *p21* of BMSCs were upregulated after irradiation, following cell cycle arrest at the G0/G1 phase. It is worth mentioning that p16 had no obvious change even at a dose of 10 Gy, which may imply that BMSC senescence caused by irradiation was not through the initiation of the p16 signaling pathway. This is consistent with the results of Kim et al.'s research (21). This may be related to the time effect of irradiation-induced cellular senescence and even to the cell type. With irreparable and irreversible damage, cells progress to early or even late stages, manifesting as mitochondrial oxidative stress, enhanced lysosomal activity, and synthesis of more SA-β-gal (30). On the basis of our results, it is fully demonstrated that irradiation could induce the senescence of BMSCs. In addition, as we all know, although senescent cells no longer proliferate, they still retain metabolic activity and secretory functions, which are characterized by the production of a variety of inflammatory cytokines, growth factors, and proteases, collectively known as SASP (26, 27). Therefore, we performed detection of a series of SASP components, including proinflammatory cytokines (*IL-6* and *TNF*-α), metalloproteinases (*MMP9* and *MMP12*), and chemokines (*PAI-1*, *IL-8*, and *CXCL12*), and the results showed increased expression and secretion of these SASP components. Studies have confirmed that SASP has deleterious effects on the behavior of neighboring normal cells and microenvironmental stability of tissues in an autocrine and paracrine transmission manner and eventually can cause tissue dysfunction and deterioration, even exerting tumor-promoting functions to accelerate proliferation and migration of cancer cells (5, 32). Compared with young mice (aged 6 mo), a subset of cells from old mice (aged 24 mo) displayed upregulation of p16 and increasing secretion of SASP components such as IL-6, IL-1α, CXCL15, and MMP9, which have profound negative effects on bone remodeling (12). In our study, we also observed that the normal osteoblasts cocultured with CM containing multiple SASP components from irradiation-induced senescent BMSCs displayed osteogenic differentiation dysfunction. This gives a hint that the accumulation of SASP from the irradiated BMSCs may play a negative role in the process of osteogenic differentiation. Likewise, it should be noted that the JAK1/STAT pathway plays an important role in regulating the production of cytokines and a lot of evidence also shows that JAK inhibitor provides a possible treatment direction for relieving aging-related tissue dysfunction (34). This is still consistent with our experimental results that the JAK1/STAT3 signaling pathway was activated and this was accompanied by an increase in SASP secretion, that JAKi treatment effectively inhibited SASP production and the expression of phosphorylated JAK1, and that the downstream phosphorylated STAT3 expression was more significantly blocked. In addition, IRIS/JAKi CM exhibited a markedly reduced ability in osteoblast differentiation and marker gene expression compared with IRIS CM (Fig. 6). Given that there were no effects on osteoblast differentiation between osteoblasts treated with Con CM and those treated with Con/JAKi CM, it is indicated that this effect was due to JAKi having effects on senescent BMSC SASP secretion but having no effect on cytokine secretion in normal cells. These findings suggest that the SASP secretion initiated by the JAK1/STAT3 pathway may play a crucial role in osteogenic dysfunction induced in irradiation-induced senescent BMSCs.

Fig. 4. Senescence phenotypes of bone marrow-derived mesenchymal stem cells (BMSCs) induced by irradiation were characterized. *A* and *B*: BMSCs at ~1×10^4 cells per well in 6-well plates were identified by the expression of senescence-associated β-galactosidase (SA-β-gal) after irradiation. Representative images (blue represents SA-β-gal-positive cells) and quantification of SA-β-gal-positive BMSCs irradiated with different doses of gamma rays are from three independent experiments. Magnification, ×100. *P* values were calculated by Student's *t* test. Results are presented as means ± SD. Significant difference in the SA-β-gal-positive rate of the 2-Gy (*$P < 0.05$), 5-Gy (**$P < 0.01$), or 10-Gy (***$P < 0.001$) group compared with the 0-Gy group. *C*: dose-dependent G0/G1 arrest of BMSC cell cycle distribution after irradiation, as detected by flow cytometry. *D*: percentage of BMSCs in different cell cycle phases. *P* values were calculated by Student's *t* test. Results are presented as means ± SD. Significant difference in the percentage of BMSCs arrested in G0/G1 of the 5-Gy (**$P < 0.01$) or 10-Gy (**$P < 0.01$) group compared with 0-Gy group. *E–G*: expression of *p53*, *p21* and *p16* was measured by quantitative RT-PCR and Western blot analyses. *H*: relative gene expression levels of seven senescence-associated secretory phenotype (SASP) components in irradiated BMSCs. The expression and production of inflammatory factors (*IL-6* and *TNF*-α), chemokines (*IL-8* and *CXCL12*), and matrix degradation enzymes [*PAI-1*, matrix metalloproteinase-9 (*MMP9*) and *MMP12*] in the radiation group were significantly higher than those in the control group. *I*: secretion of IL-6, IL-8, and MMP9 in the supernatant collected 72 h following 10-Gy irradiation of BMSCs was detected by ELISA. All data were analyzed from three independent experiments. *P* values were calculated by Student's *t* test. Results are presented as means ± SD. Significant difference in the expression and concentration of those SASP components between irradiated and nonirradiated BMSCs: *$P < 0.05$, **$P < 0.01$, ***$P < 0.001$. mRNA, messenger RNA; PE-A, phycoerythrin area. Scale bars, 100 μm (*A*).

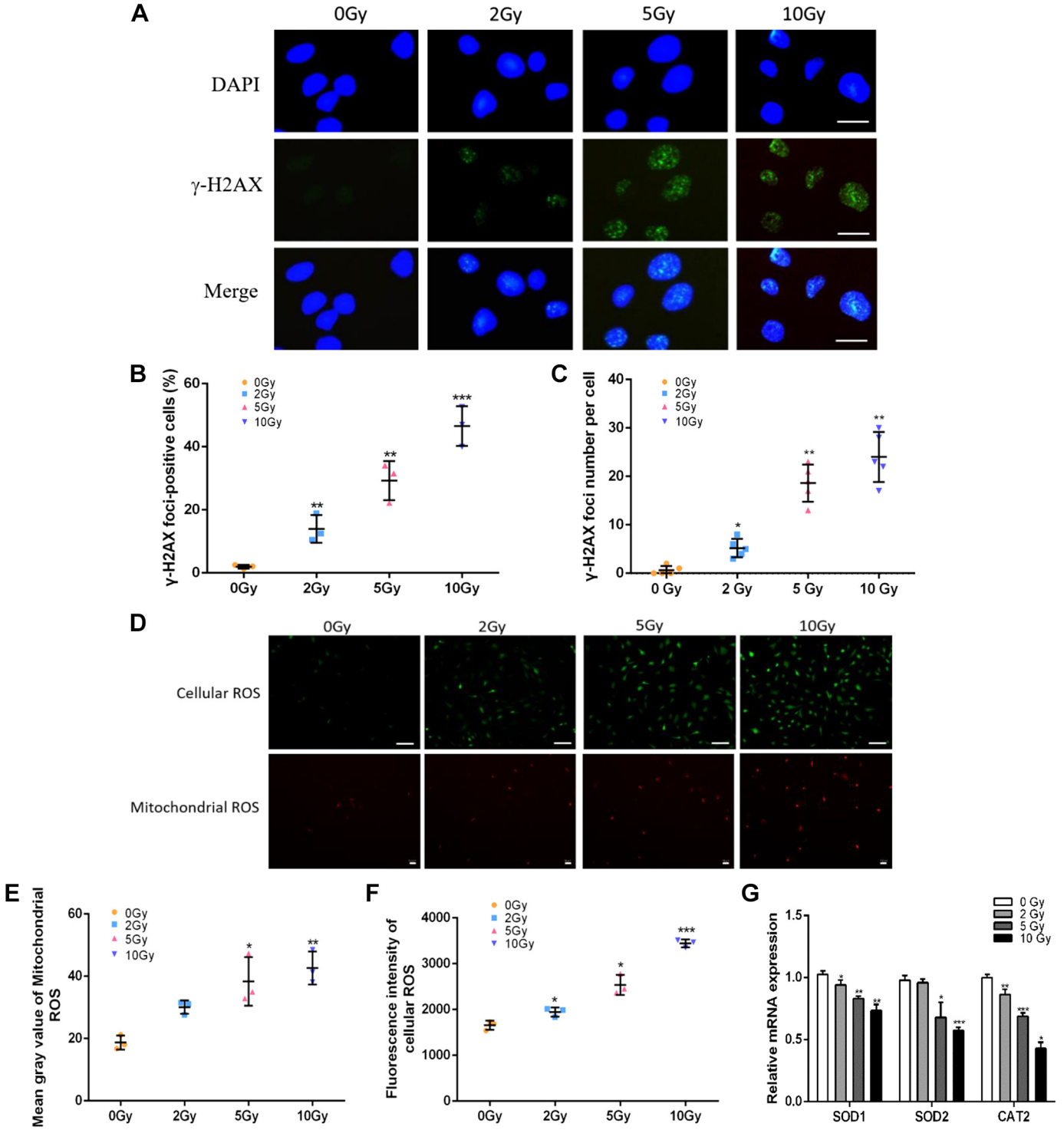

Fig. 5. Exhibition of several considerable markers associated with DNA damage and oxidative stress in irradiated bone marrow-derived mesenchymal stem cells (BMSCs). *A*: representative images of γ-H2AX immunofluorescence staining (green) and nuclei (blue) of irradiated BMSCs from three independent experiments. Magnification, ×200. *B* and *C*: percentage of γ-H2AX foci-positive (foci number >10) cells and the number of γ-H2AX foci per cell. *P* values were calculated by Student's *t* test. Results are presented as means ± SD. Significant difference in the percentage of γ-H2AX foci-positive cells and the number of γ-H2AX foci between irradiated and nonirradiated BMSCs: $*P < 0.05$, $**P < 0.01$, $***P < 0.001$. *D–F*: representative images (*D*), mean gray value of mitochondrial reactive oxygen species (ROS; *E*), and quantification of fluorescence intensity of cellular ROS (magnification, ×100; *F*) after irradiation with different doses of gamma rays. Magnification, ×100. *G*: relative messenger RNA (mRNA) expression of superoxide dismutase-1 (*SOD1*), *SOD2*, and catalase (*CAT2*) of BMSCs with irradiation and nonirradiation. All data were analyzed from three independent experiments. *P* values were calculated by Student's *t* test. Results are presented as means ± SD. Significant difference in the fluorescence intensity and expression of antioxidases between irradiated and nonirradiated BMSCs: $*P < 0.05$, $**P < 0.01$, $***P < 0.001$. DAPI, 4′,6-diamidino-2-phenylindole. Scale bars, 100 μm (*A*), 100 μm (*D*, cellular ROS), and 30 μm (*D*, mitochondrial ROS).

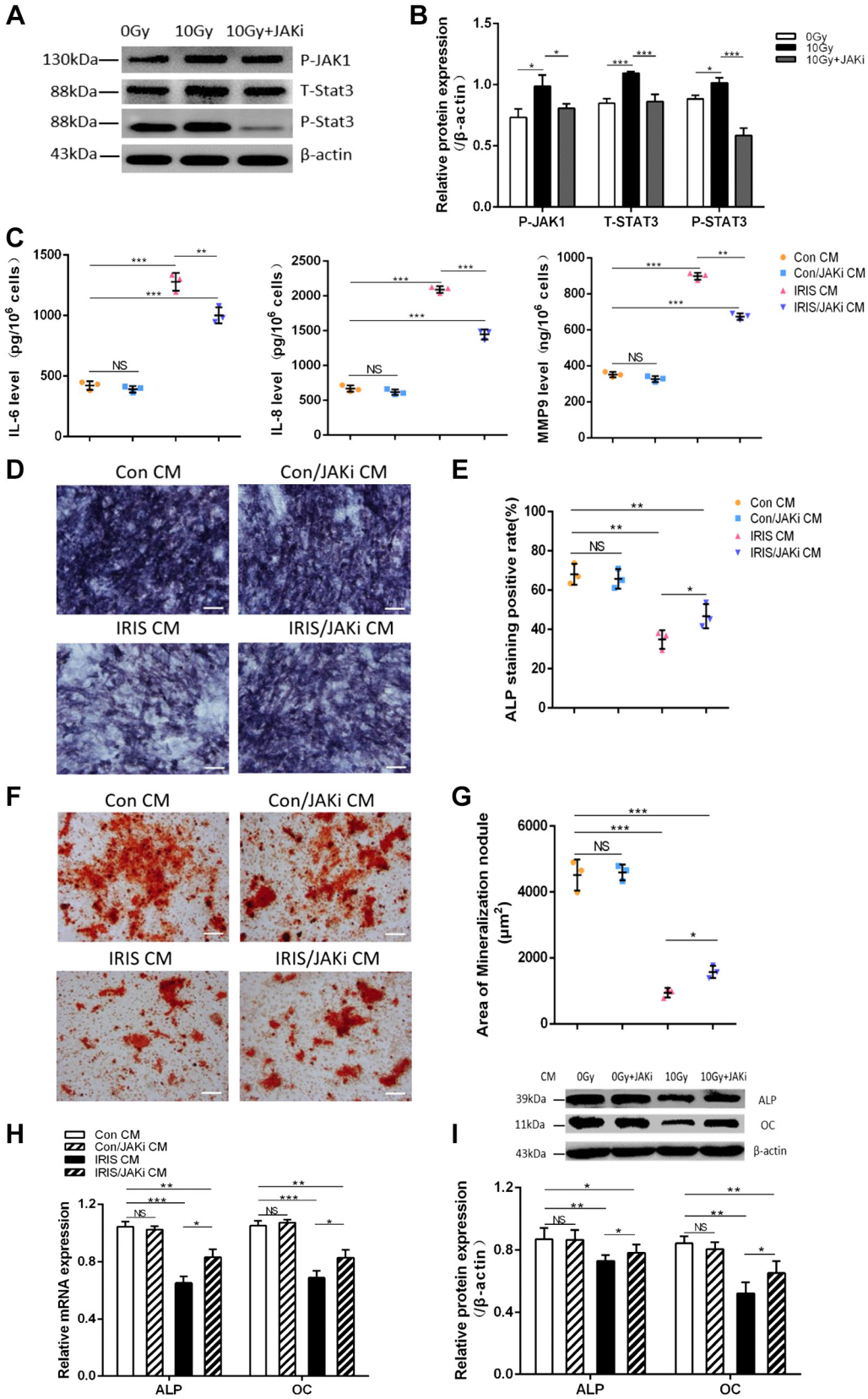

Fig. 6. Involvement of the JAK1/STAT3 pathway and the paracrine effects of irradiation-induced senescent bone marrow-derived mesenchymal stem cells (BMSCs) on osteoblast osteogenic differentiation. *A* and *B*: activation of the JAK1/STAT3 pathway after 10-Gy irradiation, as shown in Western blot analyses of phospho (p)-JAK1, total (T)-STAT3, and p-STAT3; 0.8 μM JAK1 inhibitor (JAKi) intervention could effectively inhibit the JAK1/STAT3 pathway, and the downstream p-STAT3 expression was more significantly blocked. *C*: ELISA results show upregulated secretion of IL-6, IL-8, and matrix metalloproteinase-9 (MMP9) in the supernatant collected 72 h after 10-Gy irradiation and suppressed secretion after adding 0.8 μM JAK1 inhibitor following irradiation. *D–G*: representative images and quantitative analysis of alkaline phosphatase (ALP) activity and mineralized nodule area of osteoblasts cocultured with different types of conditioned medium (CM) from irradiated BMSCs [CM from control BMSCs (Con CM), CM from control BMSCs with JAKi intervention (Con/JAKi CM), CM from irradiation-induced senescent BMSCs (IRIS CM), and CM from irradiation-induced senescent BMSCs with JAKi intervention (IRIS/JAKi CM)]. Magnification, ×100. *H* and *I*: relative messenger RNA (mRNA) and protein expression levels of *ALP* and osteocalcin (*OC*) of osteoblasts cocultured with four types of CM from irradiated BMSCs. All data were analyzed from three independent experiments. *P* values were calculated by Student's *t* test and one-way ANOVA. Results are presented as means ± SD. Scale bars, 100 μm (*D* and *F*). NS, not significant; $*P < 0.01$, $**P < 0.01$, $***P < 0.001$.

Irradiation-induced bone deterioration is not only an inevitable severe side effect of radiotherapy in patients with cancer but also a serious health problem in astronauts. Historical studies on irradiation-induced bone deterioration have focused on mechanisms of bone formation suppression and bone resorption activation, but its complex pathological mechanism has not yet been elucidated. Although antiresorption agents such as bisphosphonates and the RANK ligand inhibitor denosumab are preferred for clinical treatment of osteoporosis, the long-term use of these drugs may also cause additional bone damage, including osteonecrosis of the jaw, atypical femur fractures, and hypocalcemia (4, 37). In our study, BMSCs were first used as a carrier to explore the senescence phenotypic changes induced by irradiation. Satisfactorily, our studies preliminarily validate that senescence of BMSCs induced by radiation may be a critical mechanism of osteogenic dysfunction, and it could be a new emerging target for intervention in irradiation-induced bone loss. In addition, the results of this study can also provide a cellular senescence model for the mechanism of aging-related bone loss and clinical prevention and treatment strategy.

ACKNOWLEDGMENTS

The data that support the findings of this study are available from the corresponding author upon reasonable request.

GRANTS

This study was supported by the Natural Science Foundation of Shanghai (Grant 14ZR1401600) and the Shanghai Municipal Health Commission (Grant 20154Y0202).

DISCLOSURES

No conflicts of interest, financial or otherwise, are declared by the authors.

AUTHOR CONTRIBUTIONS

J.B., Y.W., J.W., J.Z., F.H., and G.Z. conceived and designed research; J.B., Y.W., J.W., J.Z., F.H., and G.Z. performed experiments; J.B. and G.Z. analyzed data; J.B. and G.Z. interpreted results of experiments; J.B. and G.Z. prepared figures; J.B. and G.Z. drafted manuscript; J.B., Y.W., J.W., J.Z., F.H., and G.Z. edited and revised manuscript; J.B., Y.W., J.W., J.Z., F.H., and G.Z. approved final version of manuscript.

REFERENCES

1. **Arvidson K, Abdallah BM, Applegate LA, Baldini N, Cenni E, Gomez-Barrena E, Granchi D, Kassem M, Konttinen YT, Mustafa K, Pioletti DP, Sillat T, Finne-Wistrand A.** Bone regeneration and stem cells. *J Cell Mol Med* 15: 718–746, 2011. doi:10.1111/j.1582-4934.2010.01224.x.
2. **Becerikli M, Jaurich H, Schira J, Schulte M, Döbele C, Wallner C, Abraham S, Wagner JM, Dadras M, Kneser U, Lehnhardt M, Behr B.** Age-dependent alterations in osteoblast and osteoclast activity in human cancellous bone. *J Cell Mol Med* 21: 2773–2781, 2017. doi:10.1111/jcmm.13192.
3. **Bellantuono I, Aldahmash A, Kassem M.** Aging of marrow stromal (skeletal) stem cells and their contribution to age-related bone loss. *Biochim Biophys Acta* 1792: 364–370, 2009. doi:10.1016/j.bbadis.2009.01.008.
4. **Campisi G, Fedele S, Fusco V, Pizzo G, Di Fede O, Bedogni A.** Epidemiology, clinical manifestations, risk reduction and treatment strategies of jaw osteonecrosis in cancer patients exposed to antiresorptive agents. *Future Oncol* 10: 257–275, 2014. doi:10.2217/fon.13.211.
5. **Campisi J, d'Adda di Fagagna F.** Cellular senescence: when bad things happen to good cells. *Nat Rev Mol Cell Biol* 8: 729–740, 2007. doi:10.1038/nrm2233.
6. **Chen J, Crutchley J, Zhang D, Owzar K, Kastan MB.** Identification of a DNA damage-induced alternative splicing pathway that regulates p53 and cellular senescence markers. *Cancer Discov* 7: 766–781, 2017. doi:10.1158/2159-8290.CD-16-0908.
7. **Chen X, Li M, Yan J, Liu T, Pan G, Yang H, Pei M, He F.** Alcohol induces cellular senescence and impairs osteogenic potential in bone marrow-derived mesenchymal stem cells. *Alcohol Alcohol* 52: 289–297, 2017. doi:10.1093/alcalc/agx006.
8. **de Magalhães JP, Passos JF.** Stress, cell senescence and organismal ageing. *Mech Ageing Dev* 170: 2–9, 2018. doi:10.1016/j.mad.2017.07.001.
9. **D'Oronzo S, Stucci S, Tucci M, Silvestris F.** Cancer treatment-induced bone loss (CTIBL): pathogenesis and clinical implications. *Cancer Treat Rev* 41: 798–808, 2015. doi:10.1016/j.ctrv.2015.09.003.
10. **Farr JN, Fraser DG, Wang H, Jaehn K, Ogrodnik MB, Weivoda MM, Drake MT, Tchkonia T, LeBrasseur NK, Kirkland JL, Bonewald LF, Pignolo RJ, Monroe DG, Khosla S.** Identification of senescent cells in the bone microenvironment. *J Bone Miner Res* 31: 1920–1929, 2016. doi:10.1002/jbmr.2892.
11. **Farr JN, Khosla S.** Cellular senescence in bone. *Bone* 121: 121–133, 2019. doi:10.1016/j.bone.2019.01.015.
12. **Farr JN, Xu M, Weivoda MM, Monroe DG, Fraser DG, Onken JL, Negley BA, Sfeir JG, Ogrodnik MB, Hachfeld CM, LeBrasseur NK, Drake MT, Pignolo RJ, Pirtskhalava T, Tchkonia T, Oursler MJ, Kirkland JL, Khosla S.** Targeting cellular senescence prevents age-related bone loss in mice. *Nat Med* 23: 1072–1079, 2017 [Erratum in *Nat Med* 23: 1384, 2017]. doi:10.1038/nm.4385.
13. **Gnani D, Crippa S, Della Volpe L, Rossella V, Conti A, Lettera E, Rivis S, Ometti M, Fraschini G, Bernardo ME, Di Micco R.** An early-senescence state in aged mesenchymal stromal cells contributes to hematopoietic stem and progenitor cell clonogenic impairment through the activation of a pro-inflammatory program. *Aging Cell* 18: e12933, 2019. doi:10.1111/acel.12933.
14. **Green DE, Adler BJ, Chan ME, Rubin CT.** Devastation of adult stem cell pools by irradiation precedes collapse of trabecular bone quality and quantity. *J Bone Miner Res* 27: 749–759, 2012. doi:10.1002/jbmr.1505.
15. **Hayflick L, Moorhead PS.** The serial cultivation of human diploid cell strains. *Exp Cell Res* 25: 585–621, 1961. doi:10.1016/0014-4827(61)90192-6.
16. **He F, Bai J, Wang J, Zhai J, Tong L, Zhu G.** Irradiation-induced osteocyte damage promotes HMGB1-mediated osteoclastogenesis in vitro. *J Cell Physiol* 234: 17314–17325, 2019. doi:10.1002/jcp.28351.
17. **Herranz N, Gil J.** Mechanisms and functions of cellular senescence. *J Clin Invest* 128: 1238–1246, 2018. doi:10.1172/JCI95148.
18. **Ishida T, Ishida M, Tashiro S, Takeishi Y.** DNA damage and senescence-associated inflammation in cardiovascular disease. *Biol Pharm Bull* 42: 531–537, 2019. doi:10.1248/bpb.b18-00865.
19. **Ji J, Tian Y, Zhu YQ, Zhang LY, Ji SJ, Huan J, Zhou XZ, Cao JP.** Ionizing irradiation inhibits keloid fibroblast cell proliferation and induces premature cellular senescence. *J Dermatol* 42: 56–63, 2015. doi:10.1111/1346-8138.12702.
20. **Jilka RL, O'Brien CA.** The role of osteocytes in age-related bone loss. *Curr Osteoporos Rep* 14: 16–25, 2016. doi:10.1007/s11914-016-0297-0.
21. **Kim HN, Chang J, Shao L, Han L, Iyer S, Manolagas SC, O'Brien CA, Jilka RL, Zhou D, Almeida M.** DNA damage and senescence in osteoprogenitors expressing Osx1 may cause their decrease with age. *Aging Cell* 16: 693–703, 2017. doi:10.1111/acel.12597.
22. **Krause AR, Speacht TL, Zhang Y, Lang CH, Donahue HJ.** Simulated space radiation sensitizes bone but not muscle to the catabolic effects of mechanical unloading. *PLoS One* 12: e0182403, 2017. doi:10.1371/journal.pone.0182403.
23. **Li XF, Zhu GY, Wang JP, Wang Y.** Inhibitory effects of autologous γ-irradiated cell conditioned medium on osteoblasts in vitro. *Mol Med Rep* 12: 273–280, 2015. doi:10.3892/mmr.2015.3354.
24. **Liu Z, Li T, Deng S, Fu S, Zhou X, He Y.** Radiation induces apoptosis and osteogenic impairment through miR-22-mediated intracellular oxidative stress in bone marrow mesenchymal stem cells. *Stem Cells Int* 2018: 1, 2018. doi:10.1155/2018/5845402.
25. **Lo WJ, Lin CL, Chang YC, Bai LY, Lin CY, Liang JA, Li LY, Chao LM, Chiu CF, Chen CM, Yeh SP.** Total body irradiation tremendously impair the proliferation, differentiation and chromosomal integrity of bone marrow-derived mesenchymal stromal stem cells. *Ann Hematol* 97: 697–707, 2018. doi:10.1007/s00277-018-3231-y.
26. **López-Otín C, Blasco MA, Partridge L, Serrano M, Kroemer G.** The hallmarks of aging. *Cell* 153: 1194–1217, 2013. doi:10.1016/j.cell.2013.05.039.

27. **Mária J, Ingrid Ž.** Effects of bioactive compounds on senescence and components of senescence associated secretory phenotypes in vitro. *Food Funct* 8: 2394–2418, 2017. doi:10.1039/C7FO00161D.
28. **Palmer AK, Xu M, Zhu Y, Pirtskhalava T, Weivoda MM, Hachfeld CM, Prata LG, van Dijk TH, Verkade E, Casaclang-Verzosa G, Johnson KO, Cubro H, Doornebal EJ, Ogrodnik M, Jurk D, Jensen MD, Chini EN, Miller JD, Matveyenko A, Stout MB, Schafer MJ, White TA, Hickson LJ, Demaria M, Garovic V, Grande J, Arriaga EA, Kuipers F, von Zglinicki T, LeBrasseur NK, Campisi J, Tchkonia T, Kirkland JL.** Targeting senescent cells alleviates obesity-induced metabolic dysfunction. *Aging Cell* 18: e12950, 2019. doi:10.1111/acel.12950.
29. **Sak A, Stuschke M.** Use of γH2AX and other biomarkers of double-strand breaks during radiotherapy. *Semin Radiat Oncol* 20: 223–231, 2010. doi:10.1016/j.semradonc.2010.05.004.
30. **Schafer MJ, Miller JD, LeBrasseur NK.** Cellular senescence: implications for metabolic disease. *Mol Cell Endocrinol* 455: 93–102, 2017. doi:10.1016/j.mce.2016.08.047.
31. **Tang FR, Loke WK, Khoo BC.** Postnatal irradiation-induced hippocampal neuropathology, cognitive impairment and aging. *Brain Dev* 39: 277–293, 2017. doi:10.1016/j.braindev.2016.11.001.
32. **Tchkonia T, Zhu Y, van Deursen J, Campisi J, Kirkland JL.** Cellular senescence and the senescent secretory phenotype: therapeutic opportunities. *J Clin Invest* 123: 966–972, 2013. doi:10.1172/JCI64098.
33. **Tomuleasa CI, Foris V, Soritau O, Pall E, Fischer-Fodor E, Lung-Illes V, Brie I, Virag P, Perde-Schrepler M, Postescu ID, Chereches G, Barbos O, Tatomir C.** Effects of ^{60}Co gamma-rays on human osteoprogenitor cells. *Rom J Morphol Embryol* 50: 349–355, 2009.
34. **Toso A, Revandkar A, Di Mitri D, Guccini I, Proietti M, Sarti M, Pinton S, Zhang J, Kalathur M, Civenni G, Jarrossay D, Montani E, Marini C, Garcia-Escudero R, Scanziani E, Grassi F, Pandolfi PP, Catapano CV, Alimonti A.** Enhancing chemotherapy efficacy in *Pten*-deficient prostate tumors by activating the senescence-associated antitumor immunity. *Cell Reports* 9: 75–89, 2014. doi:10.1016/j.celrep.2014.08.044.
35. **van Deursen JM.** The role of senescent cells in ageing. *Nature* 509: 439–446, 2014. doi:10.1038/nature13193.
36. **Wei RL, Jung BC, Manzano W, Sehgal V, Klempner SJ, Lee SP, Ramsinghani NS, Lall C.** Bone mineral density loss in thoracic and lumbar vertebrae following radiation for abdominal cancers. *Radiother Oncol* 118: 430–436, 2016. doi:10.1016/j.radonc.2016.03.002.
37. **Wissing MD.** Chemotherapy- and irradiation-induced bone loss in adults with solid tumors. *Curr Osteoporos Rep* 13: 140–145, 2015. doi:10.1007/s11914-015-0266-z.
38. **Yamamoto K, Nagao S, Suzuki K, Kogiku A, Senda T, Yano H, Kitai M, Shiozaki T, Matsuoka K, Yamaguchi S.** Pelvic fractures after definitive and postoperative radiotherapy for cervical cancer: a retrospective analysis of risk factors. *Gynecol Oncol* 147: 585–588, 2017. doi:10.1016/j.ygyno.2017.09.035.
39. **Zhang J, Qiu X, Xi K, Hu W, Pei H, Nie J, Wang Z, Ding J, Shang P, Li B, Zhou G.** Therapeutic ionizing radiation induced bone loss: a review of in vivo and in vitro findings. *Connect Tissue Res* 59: 509–522, 2018. doi:10.1080/03008207.2018.1439482.